

# Differential Radiometers Using Fabry–Perot Interferometric Technique for Remote Sensing of Greenhouse Gases

Elena M. Georgieva, William S. Heaps, and Emily L. Wilson

**Abstract**—A new type of remote-sensing radiometer based upon the Fabry–Perot (FP) interferometric technique has been developed at NASA’s Goddard Space Flight Center and tested from both ground and aircraft platforms. The sensor uses direct or reflected sunlight and has channels for measuring the column concentration of carbon dioxide at 1570 nm, oxygen lines sensitive to pressure and temperature at 762 and 768 nm, and water vapor (940 nm). A solid FP etalon is used as a tunable narrow bandpass filter to restrict the measurement to the gas of interest’s absorption bands. By adjusting the temperature of the etalon, which changes the index of refraction of its material, the transmission fringes can be brought into nearly exact correspondence with the absorption lines of the particular species. With this alignment between absorption lines and fringes, changes in the amount of a species in the atmosphere strongly affect the amount of light transmitted by the etalon and can be related to gas concentration. The technique is applicable to different chemical species. We have performed simulations and instrument design studies for CH<sub>4</sub>, <sup>13</sup>CO<sub>2</sub> isotope, and CO detection.

**Index Terms**—Absorbing media, atmospheric measurements, Fabry–Perot (FP) interferometers, optical interferometry, remote sensing.

## I. INTRODUCTION

**P**RECISE detection of carbon dioxide in the atmosphere is of great interest due to its impact on trapping the long wavelength radiation emitted from the Earth’s surface. There are different scenarios about the detailed causes for the global warming of the Earth’s atmosphere. The net impact of anthropogenic aerosol emissions and greenhouse gases is a complex study [1]. Recent climate models focus more on the effects of aerosol, which can absorb solar energy and warm the atmosphere. However, the indirect effects also occur when aerosols change the cloud optical properties and reflect the solar energy back into space [2]–[5]. Studies have shown that aerosol and greenhouse gas forcing are almost of the same order of magnitude [1], [3]. However, whereas the anthropogenic aerosols have short lifetime, the carbon dioxide is a long-lived

constituent. The concentrations of the principal anthropogenic greenhouse gases (CO<sub>2</sub>, CH<sub>4</sub>, and N<sub>2</sub>O) have substantially increased during the industrial period. The carbon dioxide concentration has increased by more than 95 ppmv in the last 150 years due to the emissions of the modern industrial revolution, and the mixing ratio has become 380 ppmv [6], [7]. In this same time frame, the concentration of atmospheric methane has increased by 150% from approximately 700 to 1745 ppbv [8], [9]. Although found in lower concentrations than carbon dioxide, methane is about 20 times more effective in absorbing infrared radiation. While the majority of CO<sub>2</sub> variability occurs in the lower atmosphere (~1000–800 mbar), satellite instruments measure the total atmospheric column. Since sources and sinks at the surface represent a small perturbation to the total column, a precision of better than 1% is required [10], [11]. That number comes from the transport inversion model experiments, which indicate that global column measurements with a precision of better than 1% (3 ppmv on the 380 ppmv background) on a time scale of one month is the science requirement to improve the surface flux estimates beyond the capability of the existing network [11]. The natural geographic distribution and temporal variability of CO<sub>2</sub> sources and sinks are still not well understood, and more monitoring instruments are needed to quantify the carbon dioxide dynamics and to help predict climate change [12], [13]. The water vapor concentration resulting from the evaporation of water from land and ocean is enhanced by carbon dioxide. As carbon dioxide absorbs radiative heat from the Earth’s surface (warming the atmosphere), the atmospheric water vapor increases because the warmer air can hold more water [14]. The increased water vapor leads to an increase in the greenhouse effect and further increase in temperature; the cycle is repeated until equilibrium. For climate research, high-precision (error < 5%) water vapor measurements are needed with global coverage [15], [16].

Our knowledge of atmospheric carbon processes comes from satellites (Atmospheric Infrared Sounder, SCIAMACHY onboard ENVISAT satellite [17]) and ground network measurements. The latter consists of two main sources, i.e., the long term *in situ* CO<sub>2</sub> measurement program led by the National Oceanic and Atmospheric Administration (NOAA) Climate Monitoring and Diagnostics Laboratory and the TransCom 3 transport/flux estimation experiment [18], [19]. These *in situ* measurements are very precise (uncertainties on the order of 0.1 ppm) and accurate, but are necessarily limited in time and space. Rayner and O’Brien [11] predicted that the required accuracy for monthly averaged CO<sub>2</sub> column data needs to be better than 2.5 ppmv on 8<sup>0</sup> × 10<sup>0</sup> footprint for comparable

Manuscript received September 28, 2007; revised March 13, 2008. Current version published October 1, 2008. This work was supported in part by the Instrument Incubator Program, NASA Earth Sun-System Technology Office under Grant NRA-01-OES-01 and NASA IRAD program.

E. M. Georgieva is with the Goddard Earth Science and Technology Center, University of Maryland Baltimore County, Baltimore, MD 21228 USA, and also with the NASA Goddard Space Flight Center, Greenbelt, MD 20771 USA.

W. S. Heaps is with the Instrument Systems and Technology Division, NASA/Goddard Space Flight Center, Greenbelt, MD 20771 USA.

E. L. Wilson is with the Laser and Electro-Optics Branch, NASA/Goddard Space Flight Center, Greenbelt, MD 20771 USA.

Digital Object Identifier 10.1109/TGRS.2008.921570

performance to a moderate surface network. Such a precision is difficult to achieve.

The instrument that we have developed and tested on two flight campaigns detects the absorption of CO<sub>2</sub>, O<sub>2</sub>, and H<sub>2</sub>O gases using direct or reflected sunlight [20]–[24]. The sensor makes use of two features of the Fabry–Perot (FP) interferometer to achieve high sensitivity: high spectral resolution resulting from matching the width of an atmospheric absorption feature to the instrumental band pass, and high optical throughput enabled by the simultaneous use of multiple spectral lines. For any species that one wishes to measure, this first feature is available, whereas the use of multiple spectral features can only be employed for species with suitable spectra and freedom from interfering species in the same wavelength region. The throughput of an interferometer can be as much as two orders of magnitude larger than a spectrometer with a grating with the same resolution, which means larger signals or better signal-to-noise ratio (*S/N*). Our sensor records data every 0.1 s, has high spectral selectivity, and has only one moving part (chopper), which makes it an ideal candidate for an airborne or satellite mission. It can also work as a ground-based sensor using direct light from the Sun. The current goal is to develop a precise inexpensive ground-based device sensitive enough to measure column-averaged CO<sub>2</sub> and suitable for wide deployment as a validation instrument for the Orbiting Carbon Observatory (OCO) satellite [25]–[28]. This will fill the gaps of the sparse ground network and help to understand the global distribution of CO<sub>2</sub> and its role in climate change. Parallel to that, we are developing a new sensor for methane detection and working on simulations for systems to measure CO and <sup>13</sup>CO<sub>2</sub> isotope.

II. DESCRIPTION OF INSTRUMENT AND BASIC THEORY

The incoming light is split into three wavelength bands with a dichroic beam splitter and directed into CO<sub>2</sub>, O<sub>2</sub> pressure-sensitive, and O<sub>2</sub> temperature-sensitive channels. The optical schematic for the CO<sub>2</sub> channel of the FP instrument is shown in Fig. 1. In this design, the incoming light is focused onto a 2-mm-diameter aperture to define the field of view (FOV). The light is modulated at ~400 Hz with a chopper and then recollimated as it emerges from the aperture. The incident light in the CO<sub>2</sub> channel is prefiltered at a central wavelength of 1570 nm. The light then splits between the FP and Reference subchannels with 90% of the light going to the FP subchannel. In the FP subchannel, the light passes through the FP etalon mounted in a temperature-controlled oven for fine free spectral range (FSR) tuning. By adjusting the temperature of the etalon, which changes the index of refraction of its material, the transmission fringes can be brought into nearly exact correspondence with the absorption lines of the particular species (Fig. 2). A set of off-axis parabolic (OAP) gold mirrors focuses light onto InGaAs detectors for the CO<sub>2</sub> subchannels and Si detectors for the two oxygen channels. For bringing light into the instrument, we use fiber bundles, which intentionally scramble the incident light to remove spatial information. The FP etalons in this instrument are solid-fused silica etalons, and they have different thicknesses for each instrument channel. For the CO<sub>2</sub> channel, the etalon has an FSR of 0.306 nm, a refractive index of 1.443 at λ = 1571 nm, and a clear aperture

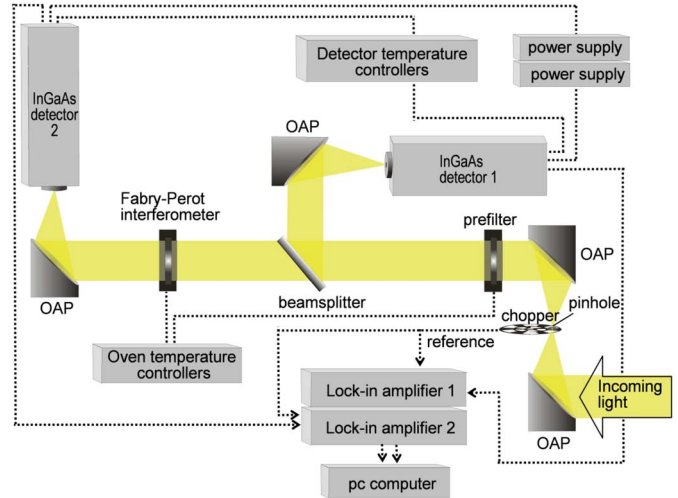


Fig. 1. Optical and electronic schematic for the CO<sub>2</sub> channel of the FP instrument. Incoming light is collimated by two OAP gold mirrors. The light is divided into FP (detector 2) and reference (detector 1) subchannels, measuring changes in CO<sub>2</sub> absorption and solar flux, respectively. The ratio of these signals can then be related to changes in the CO<sub>2</sub> column.

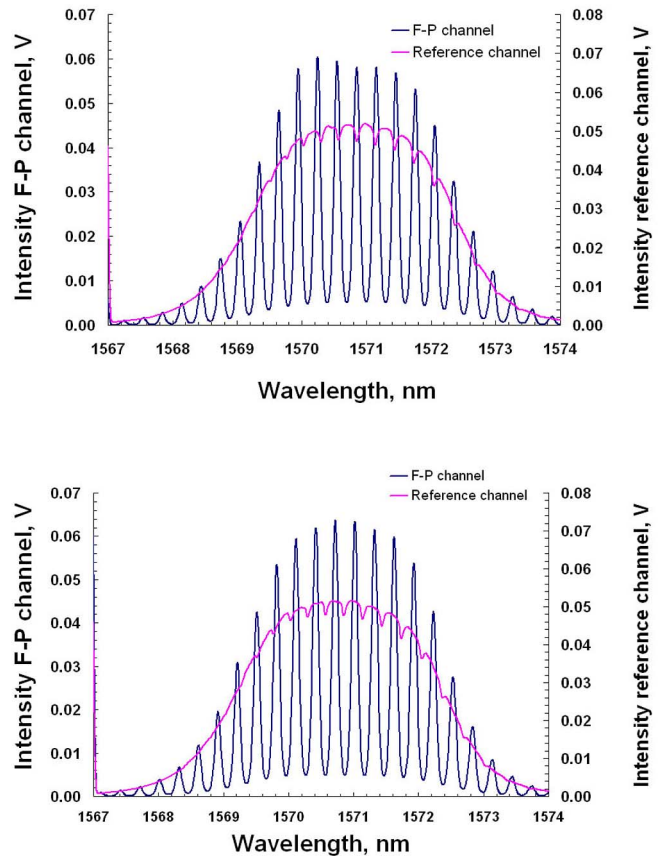


Fig. 2. Alignment of etalon transmission bands (blue) with CO<sub>2</sub> absorption lines (pink) can be adjusted by changing the etalon temperature. An etalon temperature of 54 °C (top) shows better alignment than at 42 °C (bottom).

of 50 mm with highly reflective coatings on both surfaces. The light that passes through the etalon undergoes multiple reflections on each inside surface, creating an interference pattern of equidistant fringes as a function of frequency. The width of the

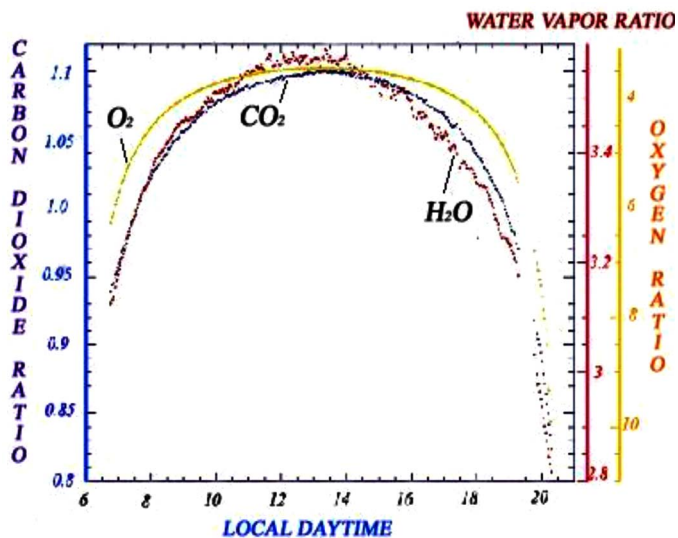


Fig. 3. FP to Reference channel ratio is plotted as a function of local time for an O<sub>2</sub> instrument (yellow), a CO<sub>2</sub> instrument (blue), and a water vapor instrument (red). The principal variation is that arising from the change in air mass as the sun rises and sets throughout the day. The measurement is done on June 30, 2006, and data were collected every 0.1 s and averaged for every 120 s.

pass bands depends on the coatings quality and on the flatness and parallelism of the surfaces. The Fresnel formalism gives the reflected and transmitted amplitude components for the light wave as functions of the optical constants of the two media and the angle of incidence. The resulting intensity follows the Airy function distribution pattern. The ideal FP etalon with perfectly flat surfaces transmits a narrow spectral band, and the energy transmission coefficient  $I_T$  is given by [29], [30]

$$I_T = \frac{T^2}{(1 - R)^2} \left[ 1 + \frac{4R}{(1 - R)^2} \sin^2 \left( \frac{2\pi n d \cos \theta}{\lambda} \right) \right]^{-1} \quad (1)$$

where  $\lambda$  is the wavelength,  $n$  is the refractive index,  $d$  is the thickness of the etalon,  $\theta$  is the angle of incidence within the cavity,  $T$  is the intensity transmission coefficient for each coating, and  $R$  is the intensity reflection coefficient. The transmission is periodic.

### III. EXPERIMENTAL

#### A. Data Taken With the Flight Version of the FP Radiometer

Carbon dioxide and oxygen column measurements using the FP radiometer have been demonstrated in laboratory, ground-based, and airborne experiments. Water vapor channel was recently added and has been tested in the lab and ground-based measurements. The FP radiometer is taking daily measurements at Goddard as a ground-based sensor, and the CO<sub>2</sub>, O<sub>2</sub>, and H<sub>2</sub>O columns are measured through absorption of light by those species in the atmosphere directly between the sun and the instrument. We accomplished this by collecting light with a small telescope fixed to an equatorial mount, aligned to track the sun throughout the day. An optical fiber coupled at the rear of the collimator brings light into the instrument. The initial tests indicate that the instrument can detect changes in the CO<sub>2</sub> column as small as 2.3 ppm with a 1 s average and better

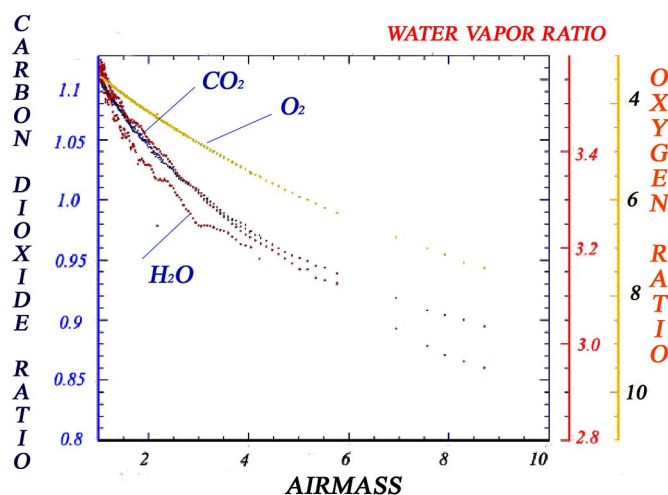


Fig. 4. Here, the ratios from the previous figure are plotted against the calculated air mass. The A.M. and P.M. values for O<sub>2</sub> are virtually the same and cannot be distinguished. The CO<sub>2</sub> channel shows some slight variation throughout the day, probably arising from consumption by plants. The water vapor channel shows considerable variation consistent with typical changes in humidity throughout a day.

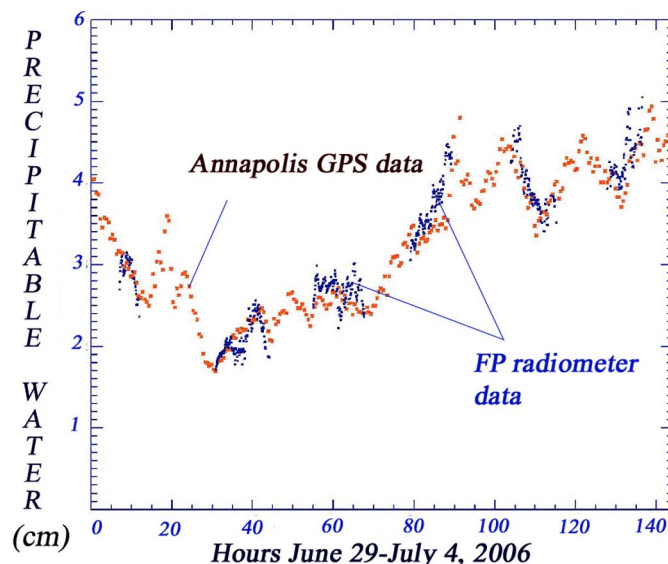


Fig. 5. Water vapor data taken on June 29, 2006 at Goddard using FP radiometer (blue dots) compared to Annapolis water vapor data (red dots). The FP radiometer data and the NOAA data using GPS technology show remarkable agreement.

than 1 ppm in less than 10 s of averaging. The precision of the oxygen column pressure changes is as small as 0.88 mbar. The water vapor precision is 2% for 1 s of averaging. Fig. 3 illustrates a typical data set collected over the course of a clear day with the instrument. The ratio of FP to reference signals is inversely proportional to absorption for CO<sub>2</sub> and H<sub>2</sub>O, and directly proportional for O<sub>2</sub>, which is plotted on an inverted scale. Fig. 4 shows the same data plotted as a function of the calculated air mass (the path length of the sunlight through the atmosphere between the sun and the instrument). The air mass decreases all morning until local noon and then increases until sunset. The air mass  $m$  is expressed by the Chapman function in the Interactive Data Language program for data analysis, so

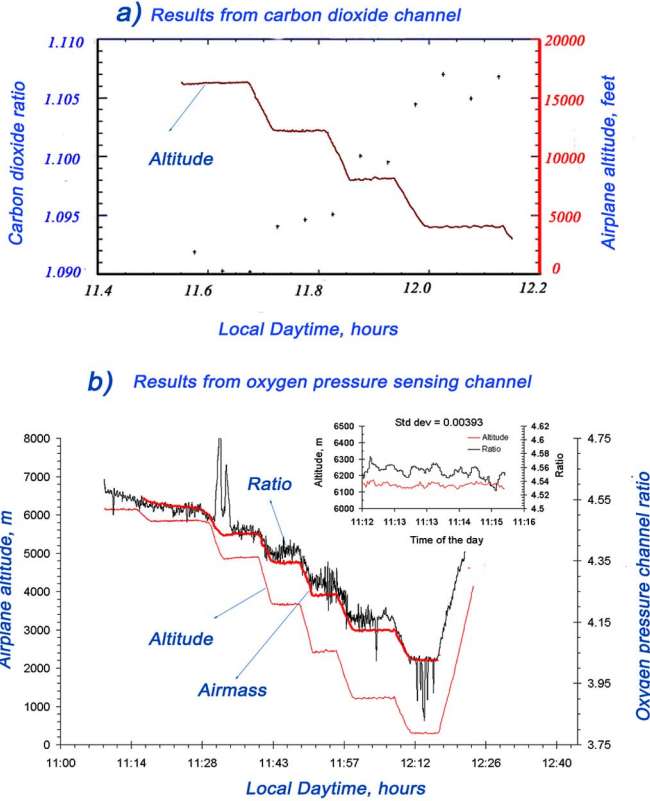


Fig. 6. Instrument response to altitude in meters at airborne mission. (a) CO<sub>2</sub> ratio of FP to Reference signals is shown compared to changes in altitude on a May 14, 2004 flight. As the aircraft descends, the photon path length gets shorter so the absorption in the FP subchannel decreases. (b) Ratio for the pressure-sensing channel (O<sub>2</sub>) and air mass as a function of time is shown. The embedded graph shows the blown images of the measured Ratio and altitude for 4 min. The standard deviation is calculated to be 0.00393.

we can account for the sphericity of the Earth as

$$m_i = \frac{1}{\tau_i} \int_{z_0}^{\infty} \sigma_i(z) \frac{dz}{\left[1 - \left(\frac{n_0 z_0}{nz} \sin \theta_0\right)^2\right]^{1/2}} \quad (2)$$

where  $m$  is the air mass,  $\tau$  is the optical depth,  $\sigma$  is the extinction coefficient as a function of altitude  $z$ ,  $\theta$  is the zenith angle of the sun, and  $n$  is the atmospheric index of refraction. For very small solar zenith angles, the air mass is equal to the secant of the zenith angle, and that is the plane-parallel approximation.

The O<sub>2</sub> data essentially lie on top of one another because the atmospheric pressure (and hence the O<sub>2</sub> column) was constant on this day. The CO<sub>2</sub> channel shown in blue has some slight variability. CO<sub>2</sub> is expected to very slightly change on a diurnal basis because of the consumption of CO<sub>2</sub> by plants during the day. CO<sub>2</sub> also has a seasonal variability with maxima in spring and minima in the late summer [31]. Those variations reflect changes in the biological sinks and can range from 1 ppmv in the Southern Hemisphere to more than 20 ppmv in the Northern Hemisphere.

The variation in the water vapor column is shown to be real in a comparison with the total column measurements by NOAA using Global Positioning System (GPS) technology. This result verifies that instruments of this type properly function and

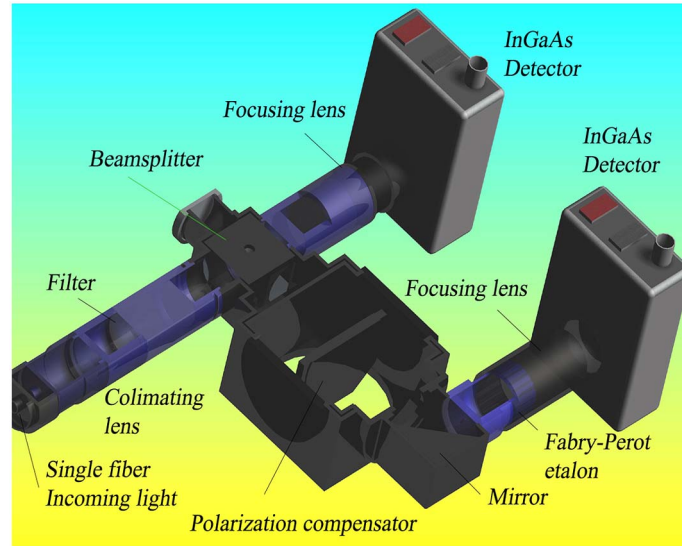


Fig. 7. Representation of the physical design of the small-size CO<sub>2</sub> instrument.

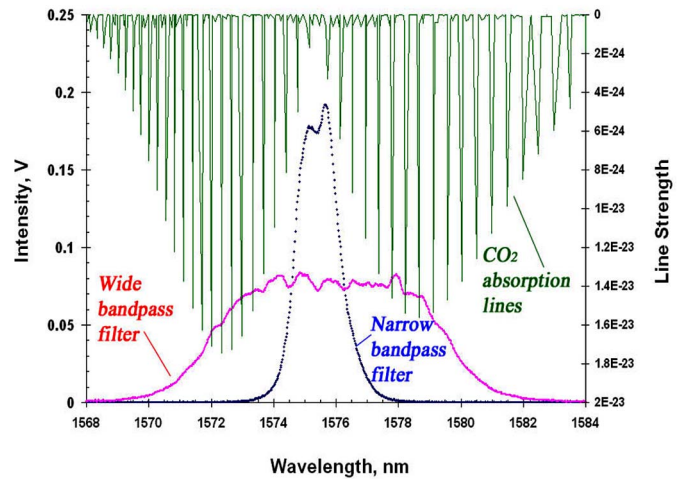


Fig. 8. Laser scan of the two filters for the small CO<sub>2</sub> radiometer. The CO<sub>2</sub> absorption lines from the HITRAN database are also shown. The narrow band versus wide band subchannel ratio will be sensitive to CO<sub>2</sub> changes in the atmosphere.

can precisely be calibrated. Fig. 5 shows this intercomparison of H<sub>2</sub>O measurement by the FP instrument system and by a NOAA GPS-based sensor located in Annapolis, MD, for five days in late June and early July. The FP radiometer only operates during the day. Agreement is consistent with the variability expected for sites ~30 miles apart.

For airborne or satellite measurements, the light passing through the atmosphere reflects on the Earth's surface before entering the instrument platform. The flight-hardened version of the instrument was tested at two flight campaigns at the National Aeronautics and Space Administration (NASA) Dryden Research Center and at New Hampshire for the Polar Aura Validation campaign on NASA's DC-8 research airplane. Flights were conducted over a variety of surfaces (vegetation, water, and snow) and under different atmospheric conditions. An *in situ* instrument provided CO<sub>2</sub> profiles up to the flight altitude. Temperature and density profiles were available from

TABLE 1  
 INSTRUMENT PARAMETERS. THE OPTICAL APERTURE FOR THE AIRBORNE FP RADIOMETER (FIG. 1) IS 0.051 m. FOR THE SMALL VERSION FP (FIG. 8), THE SIZE IS REDUCED TO 0.025 m. THE FOV IS 0.086 deg FOR BOTH INSTRUMENTS. THE DIMENSIONS OF THE AIRBORNE FP RADIOMETER ARE  $0.72 \times 0.35 \times 0.35$  m, AND THE DIMENSIONS FOR THE SMALL FP RADIOMETER ARE  $0.27 \times 0.2 \times 0.09$  m

	Bandpass Filters	FSR of the FP etalons	Resolution $\Delta\lambda/\lambda$	Sensitivity
FLIGHT VERSION of the FP RADIOMETER				
Carbon dioxide (CO <sub>2</sub> ) channel	1567-1574 nm	0.306 nm	13898	2.3ppm in 1 sec for direct light, 2% for reflected
Oxygen (O <sub>2</sub> ) pressure channel	760-764 nm	2.212 nm	2422	0.88 mbar
Oxygen (O <sub>2</sub> ) temperature channel	767-771 nm	0.575 nm	4366	0.4 deg
SMALL VERSION of the FP RADIOMETER				
Water vapor (H <sub>2</sub> O) channel	917.7-1101 nm & 925-970 nm	Bandpass filter, holographic notch filter		2% for 1 sec
Carbon dioxide (CO <sub>2</sub> ) channel	1568-1584 nm & 1573.5-1578 nm	Bandpass filters		Under test
Methane (CH <sub>4</sub> ) channel	1634-1644 nm	2.6 nm	6559	Under test
Carbon isotope ( <sup>13</sup> CO <sub>2</sub> ) channel	2111-2121 nm	0.4227 nm	42000	Under test

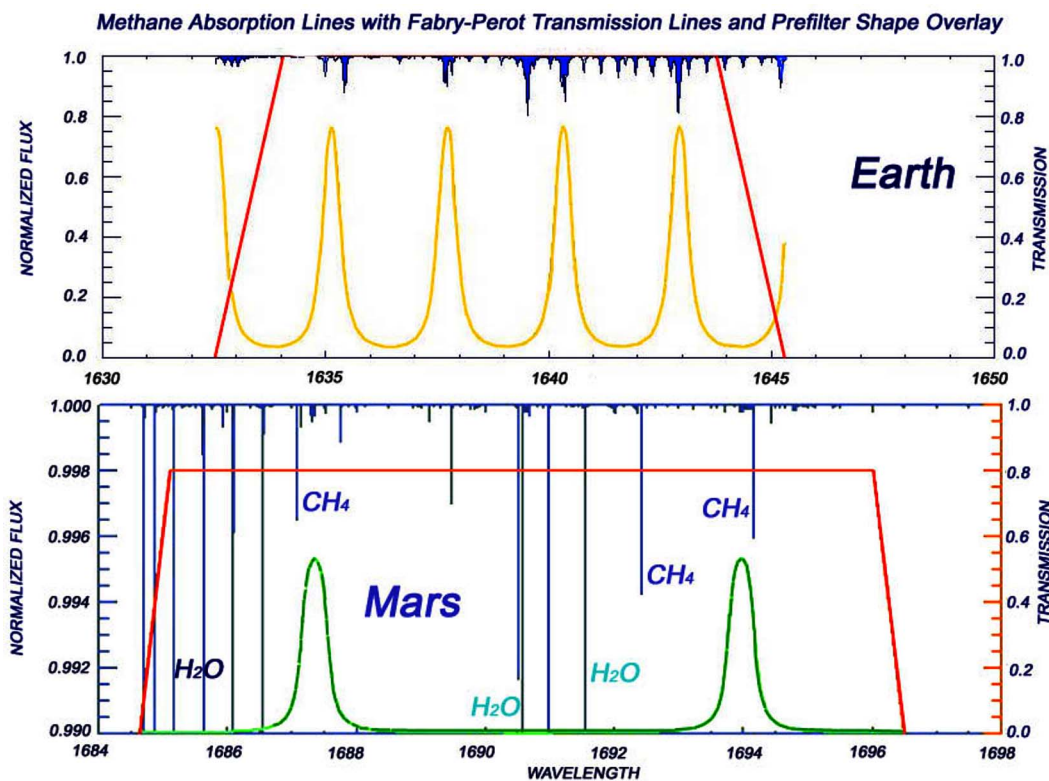


Fig. 9. Transmission bands of the solid FP etalons (yellow and green) and pass bands of the narrow prefilters (red) are shown. The top picture is representing the model simulations for the Earth atmosphere and the bottom picture for the Mars atmosphere. The absorption features of CH<sub>4</sub> are correspondingly weaker. The FP transmission bands are shown aligned with some CH<sub>4</sub> lines. There is also a strong absorption from water vapor (H<sub>2</sub>O) that can be cancelled by positioning of the etalon and the prefilter.

the aircraft data system. Comparison of FP radiometer data at different altitudes with the integrated *in situ* profiles formed the basic measure of the remote-sensing sensitivity and provided a reference calibration. Data for the airborne tests were collected, viewing in the nadir direction. Simultaneous measurements of carbon dioxide and oxygen are shown in Fig. 6(a) and (b). In both plots, the ratio of FP to Reference signals is compared to the altitude of the plane, corresponding to changes in the

total path length of sunlight through the absorber. For the CO<sub>2</sub> channel, the ratio of FP to Reference signals (blue) is inversely proportional to the column of CO<sub>2</sub> measured and, consequently, the altitude from which measurements are made (red). As expected, changes in ratio clearly track changes in altitude. We have used the change in ratio with altitude to estimate the instrument response. We obtained a value of  $-0.44$  for the change in ratio divided by the change in total column—indicating a

ratio change of approximately 40% for a change of one air mass. Improvements to the instrument since this time have increased this value. Results from the flight experiments were reported [20], [21], [23]. The airborne instrument using light reflected off the ground has a 2% precision. The precision for the airborne experiments is reduced because the aerosol and cirrus scattering significantly alter the sunlight path through the atmosphere and hence the spectral attenuation. Atmospheric scattering can produce path length changes much larger than 1%, and depending on the distribution of scattering particles and the elevation of the sun, the changes can be either positive or negative. The OCO instrument under development at the Jet Propulsion Laboratory will measure the full spectrum of CO<sub>2</sub> and O<sub>2</sub>, and the data are expected to provide enough information to permit a correction for the atmospheric scattering effects. Because we use a different technique, the approach for our instrument is to employ the glint off water for the airborne measurements. Glint has two advantages—it is bright and, therefore, will dominate the weak scattering from aerosols and thin cirrus. Second, the path length is very precisely known since the viewing angle to the glint can be measured and the location of the Sun can be calculated. Theoretical simulations show that our instrument, employing the glint, is capable of measuring the CO<sub>2</sub> column with a precision better than 0.3% for space or airborne platforms.

### B. New Sensor Design

We are in a process of developing a reduced size and volume portable channel for CO<sub>2</sub> capable of doing simultaneous measurements with the Aerosol Robotic Network at NASA, Goddard. The FP radiometer as a ground-based sensor has the potential to fill-in the sparse network of surface measurements—key in balancing the carbon budget. The instrument's low cost will enable its wide implementation to provide a broader range of intercomparison sites for the OCO instruments. For that purpose, we designed a radiometer (Fig. 7) that has a simpler configuration than the tested airborne instrument (Fig. 1). The small radiometer consists of two subchannels—the subchannel that includes very narrow bandpass filter and the subchannel that detects the total light intensity limited by the wide bandpass filter spectral range. Laser scans of the two filters are shown in Fig. 8. The CO<sub>2</sub> absorption lines from the HITRAN database are also shown. The narrow filter is fitting into the gap of the P and R branches of the CO<sub>2</sub> absorption band near 1.57  $\mu\text{m}$ . All other CO<sub>2</sub> absorption lines are blocked by the narrow filter this way. They are, however, detected by the wide filter, making it the active channel for this sensor. The sensitivity of the ground network version of the field instrument is expected to be comparable to that of the previous ground instrument. In Table I, we summarize some of the instrument parameters.

### C. Performance Simulations and Expected Results for Methane CH<sub>4</sub> and Carbon Isotope <sup>13</sup>CO<sub>2</sub> Sensors

A sensor for methane is under development. We modeled the expected performance of the instrument (Fig. 9, top) as follows. First, we generated a synthetic spectrum for reflected

light containing spectral features for CO<sub>2</sub>, H<sub>2</sub>O, and CH<sub>4</sub> from the HITRAN database [32]. Initially, we assumed an average column mixing ratio of 1.8 ppm for methane. We calculated the solar flux signal received in the two subchannels (the FP and the Reference) for light that has passed through the atmosphere and been collected by the suntracker/telescope. After perturbing the total methane column by 1%, we recalculate the signals. We compare the change in the ratio (FP/REF) caused by the perturbation to the detector noise of this ratio. The free parameters of the instrument design (e.g., FP FSR, FP finesse, filter bandpass, filter edge slopes, and instrument FOV) are varied in an effort to minimize response to changes in CO<sub>2</sub> and H<sub>2</sub>O while maximizing response to CH<sub>4</sub>. In the 1.6- $\mu\text{m}$  region, CH<sub>4</sub>, CO<sub>2</sub>, carbon monoxide (CO), and H<sub>2</sub>O have significant absorption features. Our radiometer design is based on the attempt of increasing the signal for CH<sub>4</sub> and reducing that for other interfering species. It will have the capability of measuring CH<sub>4</sub> in both the Earth and Mars environment. For CH<sub>4</sub> measurements on Mars, the thickness of the solid etalon is calculated to be 0.15 mm, the FSR is 6.6 nm, and the prefilter will be 11.4 nm wide. For the Earth measurements, the solid etalon will have 0.359-mm thickness, FSR = 2.6 nm, and the prefilter will be 11.5 nm wide. On Earth, only water vapor has significant abundance in the same spectral region. For a column average methane of 1.8 ppm and of 5000 ppm for water vapor, this instrument has a theoretical signal-to-noise ratio of 1200 : 1 for methane and less than 1 : 1 for water in a 1-s averaging period. This means that if the water vapor doubled from 5000 to 10000 ppm, it would only cause the instrument to make an error less than that arising from detector noise. Simulations for <sup>13</sup>CO<sub>2</sub> and CO were done in the same way.

## IV. CONCLUSION

We have presented a prototype passive FP-based instrument for the absorption measurements of total column carbon dioxide using sunlight at 1.58  $\mu\text{m}$ . This instrument has been demonstrated as a ground-based sensor when used in conjunction with a positioning system to follow sun movement. Signals from these data trials were found to consistently track changes in air mass. Additionally, laboratory experiments and airborne measurements validate the instrument's sensitivity to changes in CO<sub>2</sub>. Additional water vapor channel was added to the system and proved to give reasonable results. New channels for carbon monoxide (CO), methane (CH<sub>4</sub>), and carbon isotope (<sup>13</sup>CO<sub>2</sub>) are under development. The theoretical simulations for them show that sufficient S/N's can be achieved.

The FP radiometer is a mature technology for ground-based or airborne measurements capable of providing high-precision and high-spatial-resolution data of carbon dioxide, oxygen, and water vapor. It is doing rapid measurements of the entire atmospheric column, has a relatively simple design, and can use both nadir and glint viewing modes. The measurements can directly be used to validate products from a number of satellites currently operated by NASA and the European Space Agency. They can also be used as additional checks on the measurements of some of the lidar and *in situ* sensors.

ACKNOWLEDGMENT

E. M. Georgieva would like to thank B. Holben, F. S. Policelli, J. Garvin, and J. Pearl for the valuable comments they kindly provided.

REFERENCES

[1] F.-M. Bréon, "How do aerosols affect cloudiness and climate?" *Science*, vol. 313, no. 5787, pp. 623–624, Aug. 2006.

[2] Y. J. Kaufman and I. Koren, "Smoke and pollution aerosol effect on cloud cover," *Science*, vol. 313, no. 5787, pp. 655–658, Aug. 2006.

[3] M. O. Andreae, C. D. Jones, and P. M. Cox, "Strong present-day aerosol cooling implies a hot future," *Nature*, vol. 435, no. 7046, pp. 1187–1190, Jun. 2005.

[4] T. L. Anderson *et al.*, "An "A-train" strategy for quantifying direct climate forcing by anthropogenic aerosols," *Amer. Meteorol. Soc.*, vol. 86, no. 12, pp. 1795–1809, Dec. 2005.

[5] A. S. Ackerman, O. B. Toon, D. E. Stevens, A. J. Heymsfeld, V. V. Ramanathan, and E. J. Welton, "Reduction of tropical cloudiness by soot," *Science*, vol. 288, no. 5468, pp. 1042–1047, May 2000.

[6] P. J. Crutzen, "Geology of mankind," *Nature*, vol. 415, no. 6867, p. 23, Jan. 2002.

[7] J. L. Sarmiento and N. Gruber, "Sinks for anthropogenic carbon," *Phys. Today*, vol. 55, no. 8, pp. 30–36, Aug. 2002.

[8] *Climate Change 2007—The Physical Science Basis, Intergovernmental Panel on Climate Change*, Cambridge. [Online]. Available: <http://ipcc-wg1.ucar.edu/wg1/wg1-report.html>

[9] R. Beer, "TES on the Aura mission: Scientific objectives, measurements, and analysis overview," *IEEE Trans. Geosci. Remote Sens.*, vol. 44, no. 5, pp. 1102–1105, May 2006.

[10] E. Dufour and F. Breon, "Spaceborne estimate of atmospheric CO<sub>2</sub> column by use of the differential absorption method: Error analysis," *Appl. Opt.*, vol. 42, no. 18, pp. 3595–3609, Jun. 2003.

[11] P. J. Rayner and D. M. O'Brien, "The utility of remotely sensed CO<sub>2</sub> concentration data in surface source inversions," *Geophys. Res. Lett.*, vol. 28, no. 1, pp. 175–178, Jan. 2001.

[12] D. M. O'Brien and P. J. Rayner, "Global observations of the carbon budget 2. CO<sub>2</sub> column from differential absorption of reflected sunlight in the 1.61 μm band of CO<sub>2</sub>," *J. Geophys. Res.*, vol. 107, no. D18, pp. 1–16, Sep. 2002. Art. No 4354.

[13] "U.S. Global Carbon Cycle Science Program 2007," *Highlights of Recent Research and Plans for FY*, pp. 114–120, 2007.

[14] C. M. Cooney, "Uncertainties linked to water vapor's role in climate changes," *Environ. Sci. Technol.*, vol. 33, no. 23, p. 489A, 1999.

[15] V. Wulfmeyer and C. Walther, "Future performance of ground-based and airborne water-vapor differential absorption lidar. I. Overview and theory," *Appl. Opt.*, vol. 40, no. 30, pp. 5304–5320, Oct. 2001.

[16] V. Wulfmeyer and C. Walther, "Future performance of ground-based and airborne water-vapor differential absorption lidar. II. Simulations of the precision of a near-infrared, high-power system," *Appl. Opt.*, vol. 40, no. 30, pp. 5321–5336, Oct. 2001.

[17] J. R. Acarreta and P. Stammes, "Calibration comparison between SCIAMACHY and MERIS onboard ENVISAT," *IEEE Geosci. Remote Sens. Lett.*, vol. 2, no. 1, pp. 31–35, Jan. 2005.

[18] "GLOBALVIEW-CO<sub>2</sub>," *Cooperative Atmospheric Data Integration Project—Carbon Dioxide*, Boulder, CO: NOAA CMDL.

[19] K. R. Gurney, Y.-H. Chen, T. Maki, S. R. Kawa, A. Andrews, and Z. Zhu, "Sensitivity of atmospheric CO<sub>2</sub> inversions to seasonal and interannual variations in fossil fuel emissions," *J. Geophys. Res.*, vol. 110, no. D10308, pp. 1–13, May 2005.

[20] E. Georgieva, E. Wilson, M. Miodek, and W. S. Heaps, "Total column oxygen detection using Fabry–Perot interferometer," *Opt. Eng.*, vol. 45, no. 11, pp. 115001.1–115001.11, Nov. 2006.

[21] W. S. Heaps, S. R. Kawa, E. Georgieva *et al.*, "Ultra-precise measurement of CO<sub>2</sub> from space," in *Proc. Conf. Passive Opt. Remote Sens. Atmos. Clouds IV*, Nov. 2004, pp. 136–145.

[22] E. L. Wilson, E. M. Georgieva, and W. S. Heaps, "Development of a Fabry–Perot interferometer for ultra-precise measurements of column CO<sub>2</sub>," *Meas. Sci. Technol.*, vol. 18, no. 5, pp. 1495–1502, May 2007.

[23] E. M. Georgieva *et al.*, "Precise measurement of CO<sub>2</sub> from space using Fabry–Perot based optical setup: Current status and development," in *Proc. SPIE Earth Obs. Syst. XI*, 2006, vol. 6296, pp. 62961G-1–62961G-12.

[24] E. M. Georgieva *et al.*, "Atmospheric column CO<sub>2</sub> and O<sub>2</sub> absorption based on Fabry–Perot etalon for remote sensing," in *Proc. SPIE Earth Obs. Syst. X*, 2005, vol. 5882, pp. 58820G-1–58820G-9.

[25] D. Crisp and C. Johnson, "The orbiting carbon observatory mission," *Acta Astronaut.*, vol. 56, no. 1/2, pp. 193–197, Jan. 2005.

[26] D. Crisp *et al.*, "The orbiting carbon observatory (OCO) mission," *Adv. Space Res.*, vol. 34, no. 4, pp. 700–709, 2004.

[27] D. Crisp *et al.*, "The NASA orbiting carbon observatory: Measuring the column-averaged atmospheric CO<sub>2</sub> mole fraction from space," in *Proc. SPIE Sens., Syst., Next-Gener. Satell. X*, 2006, pp. U119–U128.

[28] R. Haring *et al.*, "The orbiting carbon observatory (OCO) instrument optical design," in *Proc. SPIE Curr. Dev. Lens Des. Opt. Eng. V*, 2004, pp. 51–62.

[29] J. Vaughan, *The Fabry–Perot Interferometer: History, Theory, Practice, and Applications*. Bristol, U.K.: Taylor & Francis, 1989.

[30] G. Hernandez, *Fabry–Perot Interferometers*. New York: Cambridge Univ. Press, 1986.

[31] B. Bolin, "The carbon cycle," *Sci. Amer.*, vol. 223, no. 3, pp. 124–132, Sep. 1970.

[32] L. S. Rothman *et al.*, "The HITRAN 2004 molecular spectroscopic database," *J. Quant. Spectrosc. Radiat. Transfer*, vol. 96, no. 2, pp. 139–204, Dec. 2005.



**Elena M. Georgieva** received the M.S. and Ph.D. (in 1998) degrees in physics from Sofia University, Sofia, Bulgaria.

She was a Research Associate with the Lasers and Optical Characterization Laboratory, Georgetown University, Washington, DC, where she worked on nanoparticle characterization and correlation spectroscopy. She also was a Research Associate with the NIST Center for Neutron Research and Johns Hopkins University, Baltimore, MD. For four years, she was a Senior Systems Scientist/Engineer with Science Systems and Applications and worked at the Goddard Laser and Electro-optics Branch on instrument development for the measurement of atmospheric species. She has research experience in remote sensing, data analysis and validation, instrument development, spectroscopy, interferometry, 3-D imaging laser radar system, and polarimetry. She is currently an Associate Research Scientist with the Goddard Earth Sciences and Technology Center, University of Maryland Baltimore County, Baltimore, and also with the NASA Goddard Space Flight Center, Greenbelt, MD.

Dr. Georgieva is a member of the Optical Society of America and the International Society for Optical Engineering.

**William S. Heaps** received the B.A. degree in physics from Rice University, Houston, TX, and the Ph.D. degree from the University of Wisconsin, Milwaukee, WI.

He has a long and distinguished career in atmospheric science and remote-sensing technology. His first effort was the development of a balloon-borne laser-induced fluorescence instrument that succeeded in making some of the first measurements of stratospheric hydroxyl radical. He joined the NASA Goddard Space Flight Center, Greenbelt, MD, in 1977 after a brief stint as an NRC Postdoc. In the late 1980s, he served on the mission planning group for the UARS satellite. At the same time, he developed an airborne Raman lidar system to measure water vapor and methane, and aided in the development of the Solar Disk Sextant that made the most precise ever measurements of the diameter and shape of the Sun. In 1998, he left the Atmospheric Chemistry and Dynamics Branch to become the Branch Head of the Laser and Electro-Optics Branch. While serving as Branch Head, he became the Goddard Principal Investigator for NASA's Laser Risk Reduction Program, administering more than 20 million dollars over five years in a program to enhance performance and reliability of lasers for spaceborne remote sensing. During this period, he also wrote a successful proposal to the Earth Science Technology Office's Instrument Incubator Program to begin the development of the Fabry–Perot interferometer and a successful proposal to the newly formed Office of Exploration for 3-D Laser Robot Vision. He has participated in more than 15 balloon launches. He has served as an airborne experimenter in a number of international measurement campaigns including TOTE/VOTE, SOLVE I, SOLVE II, PAVE, and INTX-B, operating lidars as well as Fabry–Perot interferometers. He currently serves as Senior Staff Engineer with the Instrument Systems and Technology Division for lasers and electrooptics.

**Emily L. Wilson** received the B.S. degree in chemistry from The University of Montana, Missoula, in 1995, the M.A. degree in chemistry from Boston University, Boston, MA, in 1999, and the Ph.D. degree in physical chemistry from The George Washington University, Washington, DC, in 2002.

From 1995 to 1997, she was a Graduate Research Fellow with Boston University, studying collisional energy transfer reactions. From 1997 to 1999, she was a Science Education Assistant with the Lemelson Center for Invention and Innovation, National Museum of American History, Smithsonian Institution, producing science education programs for middle school students. From 1999 to 2002, she was a Graduate Research Assistant with The George Washington University, conducting spectroscopic measurement of trace gases in laboratory-scale methane flames. She joined the NASA Goddard Space Flight Center, Greenbelt, MD, Laser and Electro-Optics Branch as a Physicist in 2005 following an NRC Postdoc at this branch from 2002 to 2005. She has research experience in physical chemistry, spectroscopy, and combustion, and specializes in instrument development for the measurement of atmospheric species.

Dr. Wilson was the recipient of the American Institute of Chemists Outstanding Chemistry Student Award in 1995.